Adsorption of Biebrich scarlet dye onto nano NiO and modified nano NiO: Isotherms, thermodynamic and kinetic studies

Omar Sadiq Ali
Department of Chemistry, College of Science, University of Baghdad, Baghdad, Iraq, omar.ali2105m@sc.uobaghdad.edu.iq

Dunya Edan AL-Mammar
Department of Chemistry, College of Science, University of Baghdad, Baghdad, Iraq, Dunya.almammar@gmail.com

Abstract

Present research includes the modification of the commercial nano nickel oxide NiO-C using Tetraethoxysilane (TEOS) compound. The modified nickel oxide NiO-M NPs and the commercial NiO-C NPs are both used as adsorbents to remove Biebrich Scarlet (BS) dye from water using adsorption technique. These samples were characterized using Fourier transform infrared (FTIR), X-ray diffraction (XRD, scanning electron microscopy (SEM) and Brunauer-Emmett-and-Teller (BET) to determine specific surface area and mean pore diameter. Langmuir and Freundlich adsorption isotherms were utilized and the obtained data showed that the Langmuir isotherm well described the equilibrium experimental data. Thermodynamic functions such as ΔG°, ΔH° and ΔS° were estimated and it can be indicated from this functions that the adsoption of BS dye onto NiO-M and NiO-C surfaces are spontaneous and endothermic process. The pseudo-first order (PFO) and pseudo-second order (PSO) kinetic models were used to estimate the adsorption rate, it is found that the rate mechanism explained well by the pseudo-second order model (PSO).

Keywords: *NiO-NPs; Adsorption; Biebrich Scarlet; Modification; Commercial.*

1. INTRODUCTION

Polluted water is most serious environmental problems. Continuous development in manufacturing, transportation, and urbanization, along with population increase and deforestation, is putting a constant strain on the majority of the world's freshwater supplies (Farhan et al., 2022). Dye removal from the manufacturing sector, including the food, textile, printing, and leather industries, all contributes to a serious environmental problem (Cooksey, 2020).

There are several methods for treating wastewater, including physical, chemical, and biological processes, but those currently in use have drawbacks such as poor dye removal efficiency. As a result, there is an urgent need to create alternative solutions for dealing with the problem of wastewater treatment (Ghati et al., 2017).

The adsorption technique is one of the most commonly used to remove color from wastewater. This is attributed to the dye treatment system's low cost, wide availability, simple design, high efficiency, economy, and ability to handle more concentrated colors (M. Abbas et al., 2017). Adsorption is defined as a physical or chemical bonding process arising from the bonding forces between atoms, molecules or ions of a certain substance called an adsorbate, and it may be liquid or gaseous and porous solid surfaces called adsorbent (Al Nasir and Mohammed, 2023).

Low mechanical strength and susceptibility to acidic conditions are downsides of using nanoparticles (NPs) in industry. Consequently, chemical modification was employed to provide NPs with the desired characteristics and applications. Nanoparticles fundamental structure is not altered by chemical alteration, but new variants with superior attributes are produced for specialized applications across a variety of fields. The adsorption characteristics, mechanical strength, and chemical stability of NPs in acidic conditions.(hadi and M. Al- Saadi, 2022).

Modifying NiO-NPs is under extensive study because of their potential use as environmental sorbents. The modification process has numerous advantages, including increased surface activity, physical-chemical strength, and mechanical properties (Abbas et al., 2017). Additionally, they have a high porosity, specific surface area, and may be separated from the solution to recover the costly metal phase. They are also stable at high temperatures and over a larger range of pH (Posthumus et al., 2004).

In this study, we attempted to modify a commercial NiO-NPs sample by using Tetraethoxysilane (TEOS) ($C_8H_{20}O_4Si$), then a comparison study between the commercial and modified NiO-NPs was established to remove BS dye from aqueous solutions using adsorption technique.

2. Materials and method

2.1 Materials

Commercial Nickel oxide NPs was supplied by U.S materials Co. 99.9%, Tetraethoxysilane (TEOS) from Glentham Co. 99%, pure ethanol, 0.1 M acetic acid, sodium hydroxide (0.1 M).

2.2 Modified NiO-NPs

For modification commercial NiO-NPs 3% v/v of TEOS solution in absolute ethanol was prepared. The pH solution was raised to 4-5 by adding 0.1 M acetic acid. 2 g of commercial NiO (NiO-C)were stirred with the mixture for about 10 minutes. Finally,it was left to dry for 48 hours at room temperature. The equation of reaction can be illustrated as follows (Rajeswari et al.):

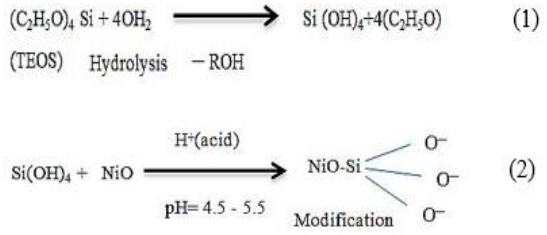

2.3. Preparation of Biebrich Scarlet (BS) dye

BS dye often known as Acid Red 66, is an anionic dye with the chemical formula $C_{22}H_{14}N_4Na_2O_7S_2$. Its IUPAC name is sodium-6-(2-hydroxynaphthylazo)-3,4-azodibenzenesulfonate. This dye is water soluble, its molar mass of 556.48 g/mol, a maximum wavelength 505 nm, and C.I. number 26905 (Onukwuli et al., 2019). Fig. 1 depicts the chemical structure of this dye.

Fig. 1: Chemical structure for BS dye

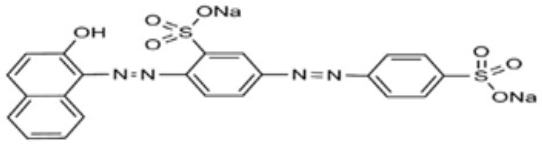

To prepare 1000 ppm from BS dye as adsorbate, one gram of BS dye was dissolved in 1000 mL of distilled water, then the stock solution was dilute to 10, 20, 30, 40, and 50 mg/L. The absorbance of the solution is determined using UV-Vis spectrophotometer.

2.4 Characterization

X-ray diffraction (XRD) pattern is investigate with anode Cu kα(λ=0.154nm) using Pan-alytical model X'pert Pro2021. Fourier transform infrared spectroscopy (FTIR) using Shimadzu model in the 4000-400 cm^{-1}

region. Brunauer-Emmett and Teller (BET) analysis carried out by using Micrometrics Gemini VII (Germany). UV-Vis spectrophotometer model (Shimadzu) was used to determine the absorption wavelength for the dye .

2.5. Equilibrium isotherm models

The BS dye uptake was assessed by two adsorption isotherm models, namely; Langmuir and Freundlich. Langmuir model described the homogenous, uniform adsorption. The linear form of Langmuir model can be expressed as(Al-Musawi and Al-Mammar, 2021).

$$\frac{C_e}{q_e} = \frac{1}{K_L . Q_m} + \frac{C_e}{Q_m} \quad (3)$$

Where q_e (mg/g) is the equilibrium amount of the substance adsorbed per gram of the adsorbent, C_e (mg/L) is the equilibrium concentration of the BS dye, K_L(L/mg) is the Langmuir isotherm constant and Q_m (mg/g) is the maximum monolayer coverage. The values of K_L and Q_m are estimated from the linear plot between C_e/q_e against C_e.

The Freundlich model describe heterogeneous surface that have different values of diffusion energy. The linear equation is written as:

$$\ln q_e = \ln k_{fr} + \frac{1}{n_f} \ln C_e \quad (4)$$

Where k_{fr} is Freundlich constant related to the adsorption capacity (mg/g)(L/mg)$^{1/n}$ and n_f is the adsorption intensity, these values were calculated from the intercept and slope of linear relation between ln q_e and ln C_e.

2.6. Thermodynamic studies

Thermodynamic parameters are essential to determining how the adsorption process occurs, either spontaneously or randomly. Thermodynamic data were estimated by the equations (Mushtaq et al., 2016, Ali et al., 2019):

$$\Delta G^o = - R\, T \ln K_{eq} \quad (5)$$

$$K_{eq} = q_e / C_e \quad (6)$$

$$\Delta G^o = \Delta H^o - T\, \Delta S^o \quad (7)$$

Where Keq equilibrium constant of the adsorption, Ci and Ce are the initial and equilibrium concentrations of the adsorbate (mg/L) respectively, m weight of the adsorbent (g), V: volume of the adsorbate (L), T absolute temperature(K) and R: universal gas constant (8.314 J.mol/K). The values of ΔS° and ΔH° can be achieved from the intercept and slope when ln Keq is plotted against 1/T according the Van't Hoff equation (Lima et al., 2020) :

$$\ln K_{eq} = \Delta S^\circ/R - \Delta H^\circ/R\, T \quad (8)$$

2.7. Adsorption Kinetic studies

The reaction pathways and the equilibrium period are provided by adsorption kinetics. To describe the adsorption process different kinetics models are applied. The pseudo-first order(PFO) model were applied for liquid / solid systems based on the solid capacitance (Yuh-Shan, 2004). It was expressed by the equation(Dunia Al-Mammar and Rawaa, 2017):

$$\ln(q_e - q_t) = \ln q_e - k_1 . t \quad (9)$$

Where q_e , q_t the adsorption capacity at equilibrium time and adsorbed amount of adsorbate at time (mg.g^{-1}) respectively, k_1 is the PFO rate constant (min^{-1}) for the adsorption process and t is the time(min). From the graph between ln (q_e-q_t) versus t it can be estimated the values of k_1 and q_e (Saxena et al., 2020). The kinetic rate equation for the pseudo-second order(PSO) model is given as (Ho, 2014) :

$$\frac{t}{q_t} = \frac{1}{K_2 . q_e^2} + \frac{t}{q_e} \quad (10)$$

Where k_2 is the equilibrium rate constant of the PSO equation (g/mg.min), k_2 and qe can be estimated from the intercept and the slope of plotting t/q_t versus t.

3. Results and discussion

3.1 Characterization of NiO−NPs adsorbents.

3.1.1. X-Ray diffraction (XRD)

XRD, the most helpful technique for phase identification, was used to evaluate the crystal and structural properties of the produced samples. Fig. 2 depicts the XRD patterns of NiO-NPs. Peaks of NiO−C sample were observed 37.47°, 43.49°, 62.12°, 75.58° and 79.65° corresponding to the same last Miller indices 111, 200, 220, 311 and 222 respectively and the reference card (JCPDS card No. 00-044-1159, it can be seen that 2 theta position for NiO−M that peak in the miller indices 220 has shifted to 63.05°, due to the modified surface (Sheshdeh et al., 2014). The crystal size (D) values for NiO-M and NiO-C samples are 23.56 and 28.14 nm, respectively, and were calculated using X'Pert HighScore software, indicating that the NiO-M sample grain size is less than the NiO-C sample due to the effect of surface modification.

Fig. 2: XRD Spectra for (a) NiO-M (b)NiO-C

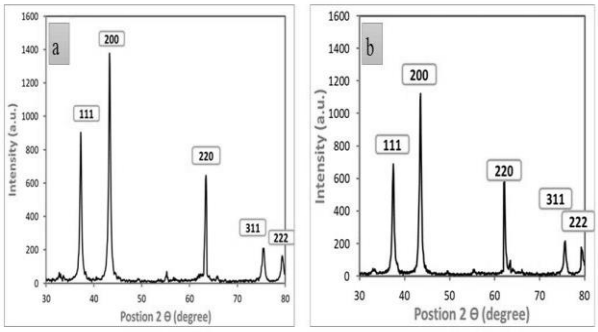

Fourier transform infrared spectroscopy(FTIR)

The FTIR spectrum for NiO-NPs samples is shown in Fig. 3 and the absorption peaks can be illustrate by Table 1.

Fig. 3: FTIR transmission for NiO−C, NiO−M samples

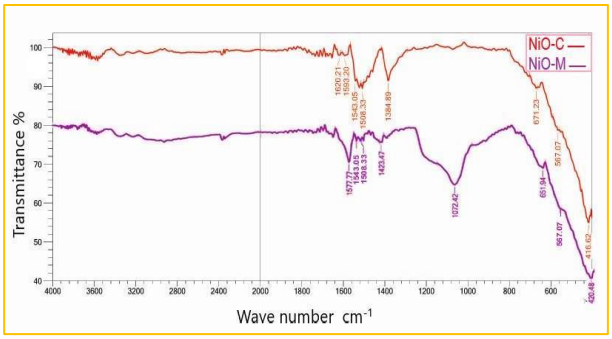

Table 1.: FTIR data

Frequency range (cm^{-1})	Functional vibration
1508 - 1620	H-O-H bending vibrations
1072	Si-O-Si group
671	Ni-O-H stretching bond
567–416	NiO bending vibrations

The peak (1072 cm-1) indicates the Si-O-Si group due to the modified surface of NiO−C (Darmawan et al., 2021).

3.1.3. Scanning electron microscopy (SEM) analysis

SEM analysis is applied to examine the surface morphology, includes size of nanoparticles distribution and shape. Fig. 4 demonstrates the SEM image for NiO−NPs samples. The particle sizes calculated using the IMAGE J software for NiO-M and NiO-C are 36.46 and 40.50 nm, respectively. NiO-M particle sizes were smaller than those in the NiO-C sample and had a spherical shape. These results match the study by Rashid I., et al. (Rashid et al., 2022).

Fig. 4: SEM images for (a)NiO-M (b)NiO-C

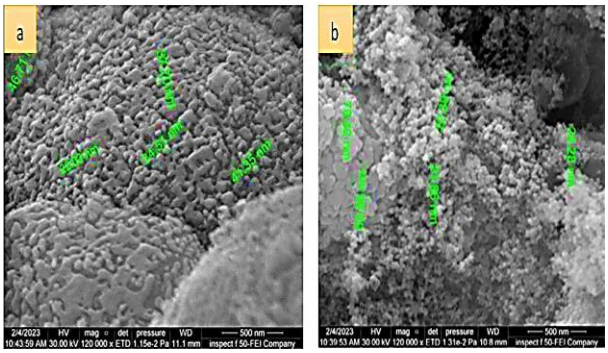

3.1.4. Brunauer–Emmett–Teller (BET) analysis

Adsorbents' surface area and pore size are two crucial factors that affected on the removal effectiveness. Fig. 5(a, b) shows the adsorption-desorption of N2 gas at 77 K that used to predict spicific surface area and porosity information using the BET analysis (Zheng et al., 2017). The values of monolayer capacity Vm is found to be 10.159 and 6.1786 cm^3/g and the spicific surface area (S_{BET}) were 44.221 and 26.895 m^2/g, while the the mean pore diameter 24.549 and 20.679 nm for NiO-M and NiO-C respictevily. The increased in these values due to the modification of the NiO−C surfaces with Si-O group.

Fig. 5: N_2 gas adsorption-desorption isotherm for(a) NiO-M, (b) NiO-C samples at 77 K

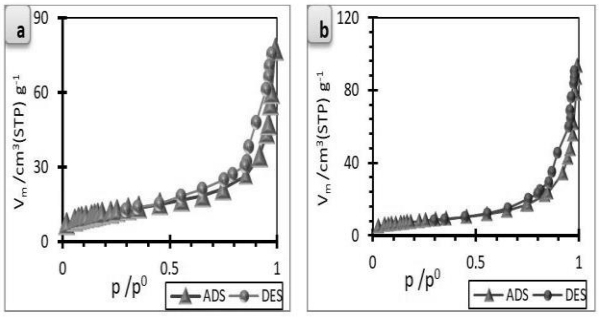

3.3 Adsorption isotherm models

3.3.1 Langmuir isotherm model

Table 2 contained the values of Langmuir constants Q_m and K_L were obtained from the as(linear plot between C_e/q_e versus C_e (Eq. 3 shown in Fig. 6.

Fig. 6: Langmuir isotherms model of BS dye adsorption onto: (a)NiO−M, (b) NiO-C.

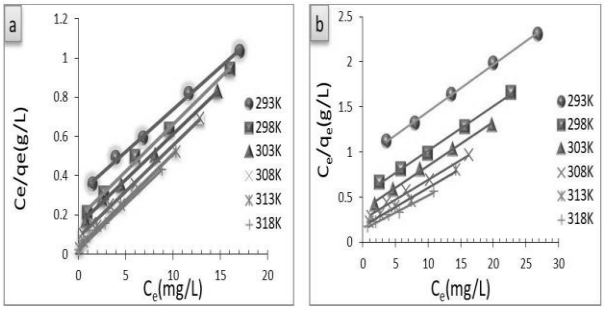

Table 2: Langmuir constants for adsorption BS dye onto NiO−NPs samples at different temperatures.

Adsorbent	Temp (K)	K_L (L/mg)	Q_m (mg/g)	R^2
NiO-M	293	0.1726	21.335	0.9987
	298	0.2286	21.491	0.9756
	303	0.3411	22.467	0.9885
	308	0.4237	24.069	0.9968
	313	0.7083	25.301	0.9871
	318	1.5471	25.966	0.9879
NiO-C	293	0.0690	18.172	0.9636
	298	0.1080	18.915	0.9747
	303	0.1025	19.281	0.9499
	308	0.1529	20.009	0.9615
	313	0.2420	21.312	0.9817
	318	0.3102	21.890	0.9855

The values of mono layer capacity Q_m for NiO-M were greater than NiO-C, this

indicated that the modification leads to enhanced the values of Q_m, due to the presence of the silican based groups. Our results agree with Al-Shammari and Al-Mammar, 2022

3.3.2Freundlich isotherm model

Fig. 7 depicts the linear plot between ln q_e versus C_e(Eq.5). The values of Freundlich constants K_{fr} and n_f are listed in Table 3, it can be seen that the values of $1/n_f < 1$, indicating that the sorption of BS dye onto NiO-NPs samples are favorable

Fig. 7: Freundlich isotherms plots for the adsorption of BS dye onto: (a) NiO−M, (b) NiO-C

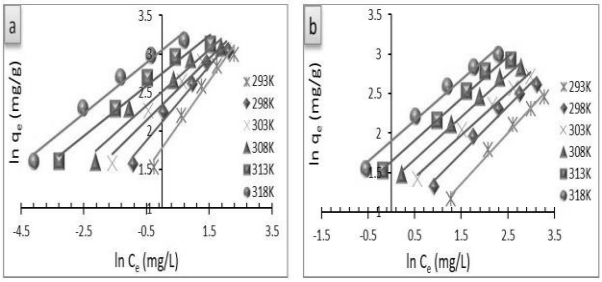

Table 3: Freundlich isotherm constants for the adsorption of BS dye onto NiO−NPs samples at different temperatures.

Adsorbent	Temp. (K)	Slope ($1/n_f$)	n_f	Intercept (ln K_{Fr})	K_{Fr} (mg/g(mg/L)$^{-1/n}$	R^2
NiO−M	293	0.5241	1.9078	1.3536	3.8716	0.9836
	298	0.4985	2.0057	1.5348	4.6406	0.9827
	303	0.4545	2.2002	1.8209	6.1777	0.9929
	308	0.5123	1.9519	2.0139	7.4925	0.9772
	313	0.4952	2.0193	2.3109	10.083	0.9048
	318	0.5698	1.7549	2.5402	12.683	0.8348
NiO−C	293	0.5992	1.6687	0.5608	1.7521	0.8961
	298	0.5858	1.7069	0.8735	2.3953	0.9101
	303	0.5547	1.8026	1.0843	2.9576	0.9835
	308	0.5715	1.7495	1.3401	3.8197	0.9705
	313	0.5383	1.8576	1.6602	5.2604	0.9677
	318	0.4997	2.0011	1.9435	6.9832	0.9110

From the values of correlation coefficient obtained for these two models, it can be noticed that Langmuir model nearly explained the applicability of the adsorption data and the adsorption of BS dye onto both adsorbents followed the mono-layer adsorption model.

3.4. Adsorption thermodynamic parameters

Fig. 8 shows the Van't Hoff plots between ln keq against 1/T (Eq.8). The spontaneity of an adsorption process is greatly influenced by thermodynamic parameters as shown in Table 3. As a result, adsorption process was assumed to be spontaneous based on the negative values for the change in the Gibbs free energy ΔG^o at the specified temperature, however the positive values for $\Delta H°$ suggested that the process was endothermic. This may be connected to the occurrence of the sorption process, which includes both adsorption and absorption. Additionally, the positive ΔS^o values, indicate increased randomness during this process (Al-Ghouti and Da'ana, 2020). These results are similar to those obtained by Kadhim and Saleh, 2022

Fig. 8: Van't Hoff plots adsorption of BS dye onto (a)NiO−M, (b) NiO-C at various temperatures.

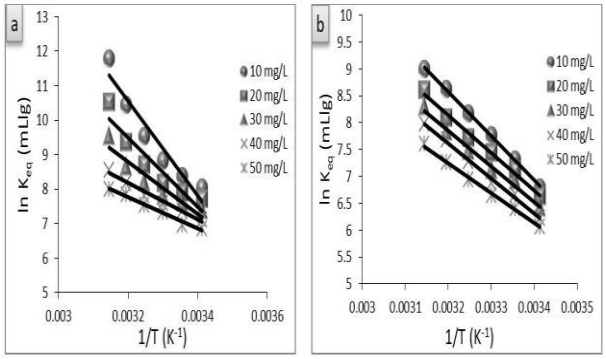

Table 4: Thermodynamic parameters for the adsorption of BS dye onto NiO−NPs samples

Adsorbent	Ci	ΔHº	ΔSº	(-)ΔGº (kJ/mol)					
	mg/L	(kJ/mol)	(J/mol.K)	293K	298K	303K	308K	313K	318K
NiO−M	10	50.033	238.25	19.584	20.745	22.687	23.482	24.653	26.383
	20	76.490	323.28	18.788	19.585	20.844	22.818	25.224	26.372
	30	70.535	300.62	18.007	18.851	20.174	21.651	23.848	25.294
	40	71.671	301.77	17.309	18.239	19.164	20.930	22.300	25.181
	50	59.084	256.88	16.615	17.217	18.364	19.922	21.417	22.823
NiO−C	10	62.278	269.81	16.839	17.942	19.575	20.769	22.432	22.844
	20	60.631	261.99	16.524	17.770	18.029	19.558	21.054	22.513
	30	59.528	256.57	15.809	17.360	17.651	19.039	20.695	21.571
	40	55.258	240.47	15.099	16.568	17.305	19.105	20.197	20.961
	50	45.405	205.45	14.988	15.656	16.774	17.780	18.948	20.022

3.5. Adsorption Kinetics

3.5.1. Pseudo-first-order (PFO) model

Fig. 9 shows the graph between ln (qe-qt) versus t (Eq.9). The values of k1, qe and R2 are shown in Table 5.

Fig. 9: PFO plots for the adsorption of BS dye onto(a)NiO-M,(b)NiO-C at different temperatures.

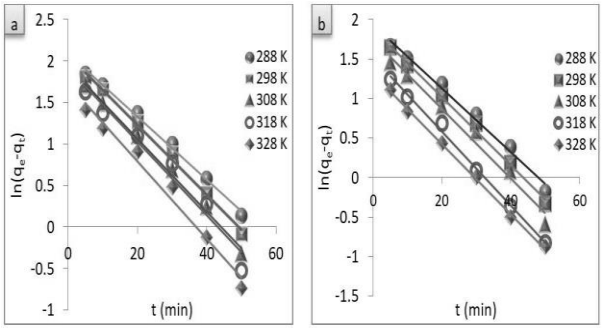

Table 5: Rate constants of PFO model for the adsorption of BS dye onto NiO−NPs samples

	NiO-M				NiO-C			
Temp. (K)	$q_{e\ exp}$ ($mg.g^{-1}$)	$q_{e\ cal}$ ($mg.g^{-1}$)	k_1 (min^{-1})	R^2	$q_{e\ exp}$ ($mg.g^{-1}$)	$q_{e\ cal}$ ($mg.g^{-1}$)	k_1 (min^{-1})	R^2
288	7.5176	5.4150	0.0302	0.8831	8.2349	6.5175	0.0318	0.8280
298	8.0997	5.8925	0.0362	0.9297	8.4428	5.8532	0.0334	0.8897
308	8.2557	5.3417	0.0398	0.9809	9.1704	5.2844	0.0332	0.9538
318	9.0457	5.6890	0.0472	0.9821	9.2536	4.7560	0.0417	0.9813
328	9.6798	5.1304	0.0499	0.9933	9.4823	3.8831	0.0379	0.9803

As shown in Table 5, the calculated qe_{cal} values disagree with the experimental qe exp at different temperatures. Moreover, from the values of the correlation coefficients (R^2) at 298K are 0.9297 and 0.8897 for NiO−M and NiO−C repactively. It can be indicates that the PFO not applicable adequately in this study.

3.5.2. Pseudo-second-order (PSO) Model

Fig.10 shows the linear plot between t/q_t versus t (Eq.10),the values of qe,k_2 and R^2 listed in Table 6

Figure 10: PSO plots for adsorption of BS dye onto (a)NiO-M, (b)NiO-C at different temperatures

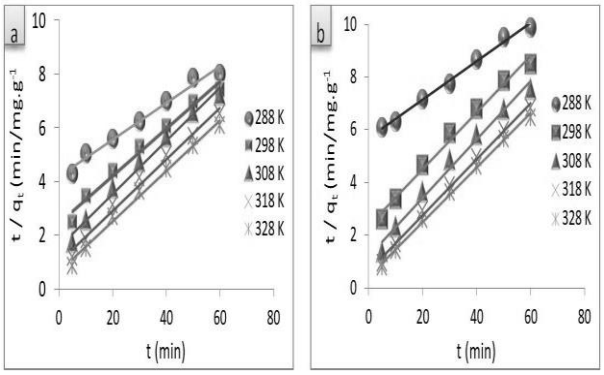

Table 6: PSO data for the adsorption of BS dye onto NiO−NPs samples at different temperatures.

	NiO−M				NiO−C			
Temp. (K)	$q_{e\ exp}$ ($mg.g^{-1}$)	$q_{e\ cal}$ ($mg.g^{-1}$)	k_2 (g/mg.min)	R^2	$q_{e\ exp}$ ($mg.g^{-1}$)	$q_{e\ cal}$ ($mg.g^{-1}$)	k_2 (g/mg.min)	R^2
288	8.3671	8.6579	0.0063	0.9629	7.5176	8.0357	0.0063	0.9010
298	8.7681	8.8130	0.0064	0.9777	8.5467	8.1834	0.0064	0.9216
308	8.9552	8.8233	0.0093	0.9902	8.2557	8.5238	0.0093	0.9730
318	9.4033	9.6281	0.0129	0.9986	9.0257	9.2183	0.0129	0.9836
328	9.6798	9.9780	0.0168	0.9979	9.0326	9.2985	0.0168	0.9857

It is clear from this Table that the values of correlation coefficient in the range of 0.9629-0.9979 and 0.9010-0.9857 for NiO-M and NiO-C repactively. Furthermore, the qe cal values are almost agreed with the experimental qe exp at all temperatures. This indicates that the PSO is a better fit for the adsorption data than the PFO.

4. Conclusions

The modification of commercial NiO-NPs with Tetraethoxysilane (TEOS) produced a sample with a high removal efficiency for adsorption BS dye. NiO-NPs samples are confirmed through various techniques. The Langmuir isotherm model fitted well with experimental data. The modification of NiO−NPs leads to enhanced the values of

mono layer capacity Qm, due to adsorption efficiency is directly related to surface modification. According to the adsorption thermodynamic functions ΔG˚, ΔH˚ and ΔS˚, the adsorption is an endothermic and occurs spontaneously. The results obtained through the kinetics study show that PSO is the best representation of the adsorption kinetics. Overall, the modification process gave clear results by improving the surface of the commercial nanomaterials for the adsorption of BS dye onto NiO-NPs. The NiO−M surface has shown great potential as an adsorbent than that NiO−C sample, due to its large specific surface area, which is a direct result of a high density of reactive sites that related to the presence of silica-based on the NiO-M surfaces.

Reference

ABBAS, A. M., MOHAMMED, Y. I. & HIMDAN, T. A. 2017. Adsorption of Anionic Dye from Equeous Solution by Modified Synthetic Zeolite. Ibn AL-Haitham Journal For Pure and Applied Sciences, 28, 52-68.

AL-GHOUTI, M. A. & DA'ANA, D. A. 2020. Guidelines for the use and interpretation of adsorption isotherm models: A review. Journal of hazardous materials, 393, 122383.

AL-MUSAWI, H. A. & AL-MAMMAR, D. E. 2021. Adsorption of Naphthol Green B Dye on to Ca-Montmorillonite and Nano-Composite Ca-Montmorillonite Clay. Annals of the Romanian Society for Cell Biology, 2797-2810.

AL-SHAMMARI, N. H. & AL-MAMMAR, D. E. 2022. Adsorption of Biebrich Scarlet Dye into Remains Chromium and Vegetable Tanned Leather as Adsorbents. Iraqi Journal of Science, 63, 2814-2826.

AL NASIR, H. A. & MOHAMMED, S. S. 2023. Experimental Investigation on Adsorption of Methyl orange Using eggshells as adsorbent Surface. Ibn AL-Haitham Journal For Pure and Applied Sciences, 36, 197-207.

ALI, I. H., AL MESFER, M. K., KHAN, M. I., DANISH, M. & ALGHAMDI, M. M. 2019. Exploring adsorption process of lead (II) and chromium (VI) ions from aqueous solutions on acid activated carbon prepared from Juniperus procera leaves. Processes, 7, 217.

COOKSEY, C. 2020. Quirks of dye nomenclature. 13. Biebrich scarlet. Biotechnic & Histochemistry, 95, 194-197.

DARMAWAN, A., RASYID, S. A. & ASTUTI, Y. 2021. Modification of the glass surface with hydrophobic silica thin layers using tetraethylorthosilicate (TEOS) and trimethylchlorosilane (TMCS) precursors. Surface and Interface Analysis, 53, 305-313.

DUNIA AL-MAMMAR & RAWAA 2017. Application of Surfactant for Enhancing the Adsorption of Azo Dye Onto Buckthorn Tree Wood Surface. Iraqi Journal of Science, 58, 1780-1798.

FARHAN, A. M., ZAGHAIR, A. M. & ABDULLAH, H. I. 2022. Adsorption Study of Rhodamine –B Dye on Plant (Citrus Leaves). Baghdad Science Journal, 19, 0838.

GHATI, S. K., SULAIMAN, I. D. & ABDULLA, N. I. 2017. Adsorption of Congo Red Dye from Aqueous Solution onto Natural and Modified Bauxite Clays. Baghdad Science Journal, 14, 0167.

HADI, K. & M. AL- SAADI, T. 2022. Investigating the Structural and Magnetic Properties of Nickel Oxide Nanoparticles Prepared by Precipitation Method. Ibn

AL-Haitham Journal For Pure and Applied Sciences, 35, 94-103.

HO, Y.-S. 2014. Using of "pseudo-second-order model" in adsorption. Environmental Science and Pollution Research, 21, 7234-7235.

KADHIM, H. H. & SALEH, K. A. 2022. Removing Cobalt ions from Industrial Wastewater Using Chitosan. Iraqi Journal of Science, 63, 3251-3263.

LIMA, E. C., GOMES, A. A. & TRAN, H. N. 2020. Comparison of the nonlinear and linear forms of the van't Hoff equation for calculation of adsorption thermodynamic parameters (ΔS° and ΔH°). Journal of Molecular Liquids, 311, 113315.

M. ABBAS, A., I. MOHAMMED, Y. & A. HIMDAN, T. 2017. Adsorption Kinetic and Thermodynamic Study of Congo Red Dye on Synthetic Zeolite and Modified Synthetic Zeolite. Ibn AL-Haitham Journal For Pure and Applied Sciences, 28, 54-72.

MUSHTAQ, M., BHATTI, H. N., IQBAL, M. & NOREEN, S. 2016. Eriobotrya japonica seed biocomposite efficiency for copper adsorption: Isotherms, kinetics, thermodynamic and desorption studies. Journal of Environmental Management, 176, 21-33.

ONUKWULI, O. D., OBIORA-OKAFO, I. A. & OMOTIOMA, M. 2019. CHARACTERIZATION AND COLOUR REMOVAL FROM AN AQUEOUS SOLUTION USING BIO-COAGULANTS: RESPONSE SURFACE METHODOLOGICAL APPROACH. Journal of Chemical Technology & Metallurgy, 54.

POSTHUMUS, W., MAGUSIN, P., BROKKEN-ZIJP, J., TINNEMANS, A. & VAN DER LINDE, R. 2004. Surface modification of oxidic nanoparticles using 3-methacryloxypropyltrimethoxysilane. Journal of Colloid and Interface Science, 269, 109-116.

RAJESWARI, K., RAMESH, G. & GUHANATHAN, S. SURFACE FUNCTIONALIZED NANO NICKEL OXIDE/UNSATURATED POLYESTER COMPOSITES FOR ENGINEERING APPLICATIONS.

RASHID, I., SALMAN, S., KAREEM MOHAMMED, P. & MAHDI, Y. 2022. Green Synthesis of Nickle Oxide Nanoparticles for Adsorption of Dyes. Sains Malaysiana, 51, 533-546.

SAXENA, M., SHARMA, N. & SAXENA, R. 2020. Highly efficient and rapid removal of a toxic dye: adsorption kinetics, isotherm, and mechanism studies on functionalized multiwalled carbon nanotubes. Surfaces and Interfaces, 21, 100639.

SHESHDEH, R. K., NIKOU, M. R. K., BADII, K., LIMAEE, N. Y. & GOLKARNARENJI, G. 2014. Equilibrium and kinetics studies for the adsorption of Basic Red 46 on nickel oxide nanoparticles-modified diatomite in aqueous solutions. Journal of the Taiwan Institute of Chemical Engineers, 45, 1792-1802.

YUH-SHAN, H. 2004. Citation review of Lagergren kinetic rate equation on adsorption reactions. Scientometrics, 59, 171-177.

ZHENG, Y., ZHU, B., CHEN, H., YOU, W., JIANG, C. & YU, J. 2017. Hierarchical flower-like nickel (II) oxide microspheres with high adsorption capacity of Congo red in water. Journal of colloid and interface science, 504, 688-696.